Materials Advances

ROYAL SOCIETY OF CHEMISTRY

PAPER

View Article Online
View Journal | View Issue



Check for updates

Cite this: *Mater. Adv.*, 2023, 4, 1188

# Enhanced two-step two-frequency upconversion luminescence in a core/shell/shell nanostructure†

Dongcheng Han, [abc] Shizhi Yang,*[ac] Qiang Zhao,*[d] Liangliang Zhang[e] and Yan Deng[d]

Received 18th November 2022,
Accepted 13th December 2022

DOI: 10.1039/d2ma01040b

rsc.li/materials-advances

Hexagonal-phase $NaYF_4$:Er@$NaGdF_4$:Yb@$NaYF_4$:Er core/shell/shell upconversion nanoparticles (UCNPs) were synthetized using the solvothermal method and first applied in enhancing two-step two-frequency upconversion luminescence (TSTF UCL). In comparison to $NaYF_4$:0.5%Er UCNPs, the UCL intensities and contrast of $NaYF_4$:0.5%Er@$NaGdF_4$:2%Yb@$NaYF_4$:1%Er UCNPs under 850 & 1550 nm excitation increase by about 3.4 and 2.8 times, respectively. By analyzing the TSTF UCL processes, the amplified UCL was mainly attributed to the reduction of surface quenching and the improvement of 1550 nm absorption. The designed nanostructure provides a novel strategy for studying the mechanism of TSTF UCL and would drive the adoption of UCNPs in a volumetric three-dimensional (3-D) display field.

## Introduction

Rare-earth (RE)-doped two-step two-frequency upconversion (TSTF-UC) materials have attracted great interest owing to their unique process in which invisible near-infrared light at two different wavelengths is absorbed sequentially and afterwards converted to visible light[1–4] (Fig. 1), which is now being explored for its potential use in 3-D displays,[5–11] lasers,[12–14] solar cells[15–17] and super resolution fluorescence imaging.[18] In particular, these materials with high transparency and brightness make them suitable for volumetric 3-D display.

As early as the 1920s, TSTF UCL performance was first discovered by chance.[1,2] However, owing to technique limitation,[19–23] the TSTF-UC materials were difficult to apply to a 3-D display. Zito *et al.* were the first to achieve volumetric 3-D displays in a mercury vapor host material in 1962.[24] Since then, diverse gaseous host materials have been demonstrated to be capable of 3-D displays.[25–27] Compared with gaseous host materials, RE-doped transparent bulk materials could not only provide spatial voxels but also a real physical space, so people would like to achieve a volumetric 3-D display with these materials. In 1964, Brown *et al.*[7] applied for the first volumetric 3-D display patent based on fluoride crystals doped with $Tm^{3+}$, $Yb^{3+}$, and $Ho^{3+}$. Since then, numerous TSTF-UC fluoride crystals have been gradually used for volumetric 3-D displays.[5,28–30] Particularly, Downing *et al.*[6] successfully presented a three-color 3-D display derived from $Er^{3+}$, $Tm^{3+}$ and $Pr^{3+}$ singly-doped fluoride glass under the simultaneous excitation of two intersecting laser beams, which was considered the greatest achievement of the physics in 1996. Afterwards, a research boom in RE-doped fluoride glass for 3-D displays has been established in China. For example, Hou, Chen and Sun *et al.* studied and optimized the TSTF UCL performances of RE-doped fluoride glasses and analyzed their application prospects in volumetric 3-D displays.[31–33]

However, fluoride glasses doped with $RE^{3+}$ ions are always accompanied by deep colors and poor UCL contrast, which may lead to an impure 3-D color display and low resolution.[34] In addition, restricted by the growth process, providing a large and perfect fluoride crystal is not easy.[35] Compared with RE-doped fluoride glasses, transparent colorless fluoride nanoparticle solutions can be more easily prepared. To obtain larger and higher resolution images, nanoparticle solutions are the better choice for a volumetric 3-D display. With the maturity of the fluoride nanoparticle synthesis process, recently, RE-doped UC fluoride nanoparticles with designed multilayer core/shell structures were employed as a full-color 3-D display material with high resolution by Deng *et al.*[36] The 3-D display was achieved by moving the overlapped focal point of the 808 nm C.W. beam and 980 nm pulse beam within the volume of the $NaYF_4$:Nd/Yb@$NaYF_4$:Yb/Tm@$NaYF_4$@$NaYF_4$:Yb/Ho/Ce@$NaYF_4$ nanoparticles. They overcame the problem of the low resolution of 3-D images caused by using RE-doped fluoride glasses as the 3-D display media. However, Deng presented a 3-D display

[a] *Key Laboratory of Atmospheric Optics, Anhui Institute of Optics and Fine Mechanics, HFIPS, Chinese Academy of Sciences, Hefei 230031, China. E-mail: szyang@aiofm.ac.cn*
[b] *Science Island Branch of Graduate School, University of Science and Technology of China, Hefei, Anhui 230026, China*
[c] *Advanced Laser Technology Laboratory of Anhui Province, Hefei 230037, China*
[d] *School of Environment and Energy Engineering, Anhui Jianzhu University, Hefei 230601, China. E-mail: rommel99@163.com*
[e] *Anhui Easpeed Technology Co. Ltd, Hefei, Anhui 230088, China*

† Electronic supplementary information (ESI) available. See DOI: https://doi.org/10.1039/d2ma01040b

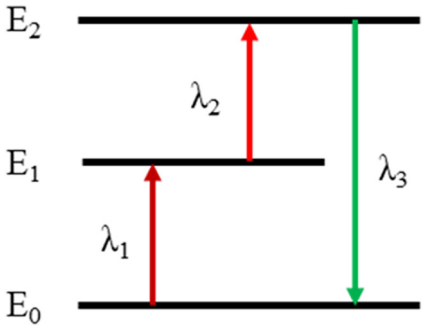


Fig. 1 Schematic illustration of the TSTF process.

based on single-frequency multiphoton UCL, which cannot present dynamic and complex 3-D images. Therefore, it is necessary to develop RE-doped TSTF UCNPs as volumetric 3-D display materials to obtain better 3-D images.

Many excellent studies on TSTF UCNPs have been reported.[37–41] For example, Chen *et al.*[37] demonstrated that enhanced UCL intensity in $NaYF_4$:1%Er nanoparticles was achieved by 790 & 1520 nm excitation. Li *et al.*[38] demonstrated that enhanced red emission in $Gd_2MoO_6$:Er/Yb nanoparticles co-doped $WO_6^{6-}$ and $La^{3+}$ was achieved by 980 & 1550 nm excitation. Guo *et al.*[39] showed that enhanced emission intensity in $GdVO_4$:Yb/Er nanoparticles doped with $Lu^{3+}$, $Y^{3+}$ and $PO_4^{3-}$ ions was achieved by 980 & 1550 nm excitation. However, TSTF UCNPs often suffer from low luminescent efficiency,[42–44] attributed to concentration quenching and surface defects,[45–50] which partly restrict further applications in the 3-D display. To enhance UCL efficiency, many approaches, such as doping sensitizers, fabricating core/shell structures, and changing the hosts, have been widely studied.[51–54] In particular, by designing core/shell structure, Chen *et al.*[55] improved the UC quantum yield to 5% in $LiLuF_4$:Yb/Er@$LiLuF_4$ UCNPs. Chen *et al.*[56] remarkably improved the UCL of $Ln^{3+}$-doped nanoparticles in $NaGdF_4$:Yb@$NaYF_4$:Yb/Er@$NaGdF_4$:Yb UCNPs.

In this study, a novel strategy is first described to improve TSTF UCL intensities and contrast *via* a designed core/shell/shell nanostructure. $Er^{3+}$-doped $NaYF_4$ was used as the luminescent core and outer luminescent shell, and $Yb^{3+}$-doped $NaGdF_4$ was used as the inner active shell. By characterization, we can conclude that controlling the distribution of $Yb^{3+}$ and $Er^{3+}$ ions can serve two purposes: (a) to protect the UCNPs from surface quenching and (b) to improve the absorption of 1550 nm. Through these two ways of enhancing TSTF UCL performances, clear volumetric 3-D images were achieved in $NaYF_4$:Er@$NaGdF_4$:Yb@$NaYF_4$:Er UCNPs solution under 850 & 1550 nm excitation.

## Experimental section

### Materials

$YCl_3{\cdot}6H_2O$ (99.99%), $GdCl_3{\cdot}xH_2O$ (99.99%), $YbCl_3{\cdot}6H_2O$ (99.9%), $ErCl_3{\cdot}6H_2O$ (99.9%), NaOH (98%), $NH_4F$ (98%), oleic acid (OA, 90%), and 1-octadecene (ODE, 90%) were purchased from Sigma-Aldrich (Shanghai, China). Ethanol, cyclohexane, and chloroform were purchased from Sinopharm Chemical Reagent Co. (Shanghai, China). All the chemical reagents were used as received without further purification.

### Synthesis of TSTF core/shell/shell UCNPs

The UCNPs were prepared by applying a solvothermal method.[57,58] The core/shell/shell UCNPs were prepared using a layer-by-layer epitaxial growth method.[59,60] $NaYF_4$:0.5%Er UCNPs were first prepared and then covered by $NaGdF_4$:2%Yb and $NaYF_4$:1%Er shell gradually (Fig. 2).

### Synthesis of $NaYF_4$:0.5%Er UCNPs

In a typical experiment, $ErCl_3{\cdot}6H_2O$ (0.005 mmol), $YCl_3{\cdot}6H_2O$ (0.995 mmol), 6 mL OA and 15 mL ODE were mixed into a 50 mL flask. The mixture was heated at 150 °C under argon flow for 30 min. After cooling to 50 °C, 10 mL of methanol solution containing 4 mmol $NH_4F$ and 2.5 mmol NaOH was added, and the solution was vigorously stirred for 1 h. Then, the slurry was slowly heated and kept at 100 °C for 10 min to remove methanol. Next, the solution was heated to 305 °C and maintained for 1 h. The resulting UCNPs were precipitated out by the addition of ethanol, collected by centrifugation, washed with a mixture of cyclohexane and absolute ethanol solvent several times, and redispersed in 4 mL chloroform.

### Synthesis of $NaYF_4$:0.5%Er@$NaGdF_4$:2%Yb UCNPs

$YbCl_3{\cdot}6H_2O$ (0.02 × 0.5 mmol), $GdCl_3{\cdot}6H_2O$ (0.98 × 0.5 mmol), 6 mL OA and 15 mL ODE were mixed into a 50 mL flask. The mixture was heated at 150 °C under argon flow for 30 min. After cooling down to 50 °C, 10 mL methanol solution containing 4 mmol $NH_4F$ and 2.5 mmol NaOH was added along with the as-prepared $NaYF_4$:0.5%Er UCNPs in 4 mL chloroform; the solution was vigorously stirred for 1 h. Then, the slurry was slowly heated and kept at 100 °C for 10 min to remove methanol. Next, the solution was heated to 305 °C and maintained for 1 h. The resulting core/shell UCNPs were precipitated out by the addition of ethanol, collected by centrifugation, washed with a mixture of cyclohexane and absolute ethanol solvent several times, and redispersed in 4 mL chloroform.

### Synthesis of $NaYF_4$:0.5%Er@$NaGdF_4$:2%Yb@$NaYF_4$:1%Er UCNPs

The procedure for preparing core/shell/shell UCNPs is the same as that for core/shell. The as-prepared core/shell UCNPs in 4 mL chloroform are used as seeds to induce subsequent epitaxial growth of an additional shell provided by $ErCl_3{\cdot}6H_2O$ ((0.01 × 0.8 mmol) and $YCl_3{\cdot}6H_2O$ (0.99 × 0.8 mmol). The resulting core/shell/shell UCNPs were dispersed in 4 mL of chloroform before characterization.

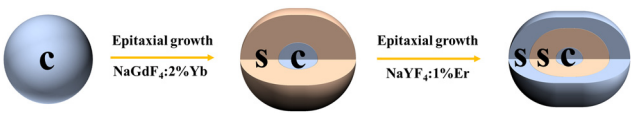


Fig. 2 Schematic procedure for the synthesis of core/shell/shell UCNPs.

### Characterization

The phase structure of the as-prepared UCNPs was investigated using an X-ray diffractometer (XRD; Bruker D8 Advance, LynxEye detector; Rigaku SmartLap, Japan) under Cu Kα radiation ($\lambda$ = 1.5406 Å) performing at 40 kV and 40 mA. The morphology and size of the as-prepared UCNPs were characterized by applying a transmission electron microscope (TEM; Hitachi HT7700 Exalens, Tokyo Japan) and scanning electron microscope (SEM; Hitachi SU8010, Tokyo, Japan). The photoluminescence quantum yield of the as-prepared UCNPs was measured using the visible-near-infrared absolute photoluminescence quantum yield test system (PLQY; C9920-02, Hamamatsu Japan). UC emission spectra were measured by employing an Aurora4000 spectrofluorometer under excitation by 850 and 1550 nm laser sources. The 850 nm laser power is maintained at 0.2 W, and the 1550 nm laser power is maintained at 0.2–2.23 W. All spectral measurements were performed at room temperature.

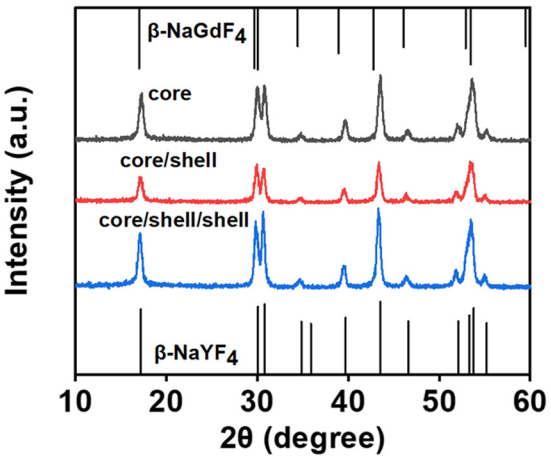


Fig. 3 XRD patterns of $NaYF_4$:0.5%Er, $NaYF_4$:0.5%Er@$NaGdF_4$:2%Yb, $NaYF_4$:0.5%Er@$NaGdF_4$:2%Yb@$NaYF_4$:1%Er UCNPs and standard date of β-$NaYF_4$ (JCPDS No. 16-0334) and β-$NaGdF_4$ (JCPDS No. 27-0699).

## Results and discussion

A novel strategy of designed core/shell/shell nanostructure was employed to enhance the TSTF UCL intensities and contrast, as shown in Fig. S1 (ESI†). $Er^{3+}$-doped hexagonal $NaYF_4$ was chosen as the host lattice of the luminescent core and outer luminescent shell because of its low phonon energies ($<400\ cm^{-1}$), low non-radiative decay rates and high radiative emission rates, which can provide high UC efficiency.[61] $Yb^{3+}$-doped hexagonal $NaGdF_4$ was chosen as the host lattice of the inner active shell for the following reasons: (a) confirmation of the successful formation of core/shell/shell structure easily. Owing to the difference in the atomic number between $Gd^{3+}$ ($Z$ = 64) and $Y^{3+}$ ($Z$ = 39), high-angle annular dark-field scanning transmission electron microscopy (HAADF-STEM) can be adopted to identify bright inner shells using image contrast. Furthermore, $Gd^{3+}$ ions can be detected using the energy dispersive spectrometer (EDS) and the electron energy loss spectrum (EELS) line scan to confirm the successful formation of core/shell/shell structure. (b) Decreasing the average crystallite size of core/shell UCNPs contributes to outer shell cladding, and promoting the phase transition from cubic to hexagonal enhances UCL intensities.[62] To illustrate that the choice of $NaGdF_4$ as the host lattice of the inner shell could improve UCL intensities, the UC emission spectra of $NaYF_4$:Er@$NaGdF_4$:Yb@$NaYF_4$:Er and $NaYF_4$:Er@$NaYF_4$:Yb@$NaYF_4$:Er UCNPs under 850 & 1550 nm and 1550 nm excitation were measured in Fig. S2 (ESI†). Compared with $NaYF_4$:Er@$NaYF_4$:Yb@$NaYF_4$:Er, the UCL integral intensities of $NaYF_4$:Er@$NaGdF_4$:Yb@$NaYF_4$:Er are greater owing to its purer hexagonal phase, which agrees with the result reported in the literature.[62]

Fig. 3 shows the crystal phase of the as-prepared core, core/shell and core/shell/shell UCNPs by applying XRD. All the XRD patterns of these samples match well with the standard JCPDS No. 16-0334 pattern of β-$NaYF_4$ and JCPDS No. 27-0699 pattern of β-$NaGdF_4$, and no significant impurity peaks were detected, indicating that all samples belong to a hexagonal-phase structure.

Fig. 4 shows the morphology and particle size of the as-prepared UCNPs by employing TEM. In Fig. 4a, $NaYF_4$:0.5%Er UCNPs have a quasi-sphere morphology. These core UCNPs are monodisperse and uniform with a mean size of 22.32 ± 0.05 nm. In Fig. 4b, the core/shell UCNPs show a uniform distribution with a short rod-like shape with an average width of 22.98 ± 0.07 nm and a length of 23.59 ± 0.04 nm. As illustrated in Fig. 4c, the rod-like shape of the core/shell/shell UCNPs dispersed well and possessed a uniform width of 24.29 ± 0.06 nm and a length of 31.88 ± 0.04 nm. The increasing size of the above UCNPs indicates that $NaGdF_4$:Yb and $NaYF_4$:Er shells were possibly covered on the surface of $NaYF_4$:1%Er UCNPs. Similar results regarding the shape of the core, core/shell and core/shell/shell UCNPs were also verified by applying SEM (Fig. S3, ESI†).

Considering the difference in atomic numbers between $Y^{3+}$ ($Z$ = 39) and $Gd^{3+}$ ($Z$ = 64) in $NaYF_4$@$NaGdF_4$@$NaYF_4$ nanostructure, HAADF-STEM was used to identify the core, core/shell and core/shell/shell by image contrast. As shown in Fig. 5, compared with $NaYF_4$, a bright $NaGdF_4$ shell can be clearly observed, which demonstrates the successful formation of core/shell/shell nanostructure. The core/shell/shell UCNPs were analyzed by applying EDS and EELS line scans to confirm their compositions (Fig. S4, ESI†). The detected $Gd^{3+}$ ions could also provide solid proof of this core/shell/shell nanostructure.

As depicted in Fig. 6, the UC emission spectra under 1550 nm and simultaneous 850 & 1550 nm excitation were shown, which was measured to compare UCL intensities ($I$) and contrast of as-prepared UCNPs. Here, the contrast is defined by $I_{850\&1550}/I_{1550}$, where $I_{850\&1550}$ and $I_{1550}$ represent the UCL integral intensities (from 500 to 700 nm). While maintaining the same doping concentration of $Yb^{3+}$ and $Er^{3+}$ ions and changing the distribution position of doping ions in different layers, we found that the UCL intensities $I_{850\&1550}$ and $I_{1550}$ of these core/shell/shell UCNPs varied significantly (Fig. 6a and b). The TSTF UCL integral intensities $I_{850\&1550}$ are described as follows: Er@Er@Yb > Er@Yb@Er > Yb@Er@Er.

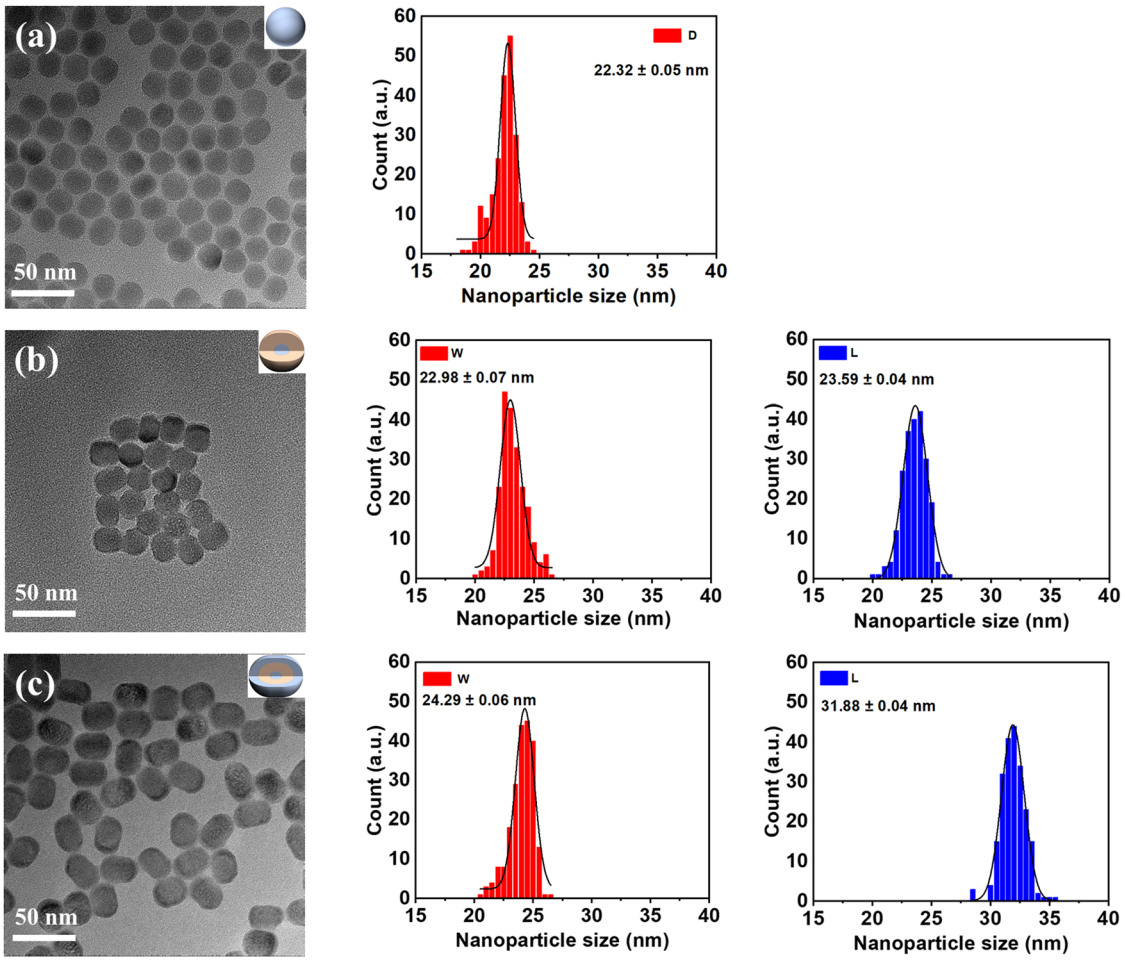


Fig. 4 TEM images of UCNPs (left) and the corresponding size distributions of UCNPs (right). (a) $NaYF_4$:0.5%Er, (b) $NaYF_4$:0.5%Er@$NaGdF_4$:2%Yb, and (c) $NaYF_4$:0.5%Er@$NaGdF_4$:2%Yb@$NaYF_4$:1%Er UCNPs. The size distributions of the UCNPs were calculated by counting over 200 particles recorded in the TEM images.

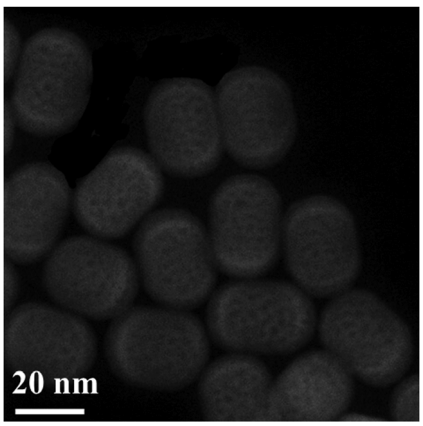


Fig. 5 HAADF-STEM images of $NaYF_4$:0.5%Er@$NaGdF_4$:2%Yb@$NaYF_4$:1%Er UCNPs.

The corresponding contrast of the above UCNPs is about 8.3, 13.5 and 3.4.

The possible reasons for the differences in the UCL intensities and contrasts of the aforementioned UCNPs are as follows. According to FRET theory, within a certain distance, the energy transfer efficiency from the luminescent center to the surface defect is inversely related to the distance between each other, namely the farther the distance is from the luminescent center to the surface defect, the less energy loss and the higher UCL intensity. Compared with the other two UCNPs, in Er@Er@Yb UCNPs, the distance from $Er^{3+}$ ions located in the core and inner shell to the surface defect is the farthest, and the TSTF UCL intensity is the highest. In Yb@Er@Er UCNPs, the distance from $Er^{3+}$ ions located in the inner and outer shell to the surface defect is the closest, and the TSTF UCL intensity is the weakest. At 1550 nm excitation, the single-frequency UCL of Er@Yb@Er UCNPs is mainly generated by $NaYF_4$:0.5%Er core UCNPs, which caused a weak UCL intensity. However, the single-frequency UCL of Er@Er@Yb UCNPs is mainly generated by $Er^{3+}$ ions in the core and inner shell, which caused a strong UCL intensity, but a decreased contrast.

The best UCL performances appeared in $NaYF_4$:Er@$NaGdF_4$:Yb@$NaYF_4$:Er (Fig. 6c). By optimizing the doping ratio of $Er^{3+}$ and $Yb^{3+}$ ions in the above nanostructure, as shown in Fig. S5 (ESI†), UCNPs with 0.5 mol% $Er^{3+}$ in the core, 2 mol%

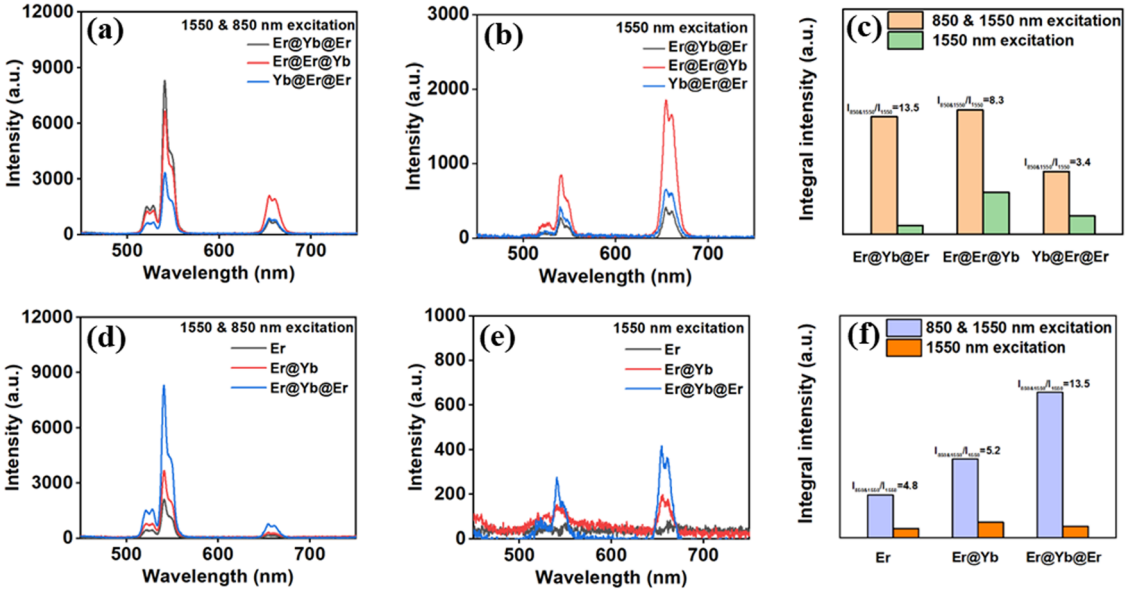


Fig. 6 UC emission spectra of $NaYF_4$:Er@$NaGdF_4$:Yb@$NaYF_4$:Er (Er@Yb@Er), $NaYF_4$:Er@$NaGdF_4$:Er@$NaYF_4$:Yb (Er@Er@Yb) and $NaYF_4$:Yb@$NaGdF_4$:Er@$NaYF_4$:Er (Yb@Er@Er) UCNPs under (a) 850 & 1550 nm, (b) 1550 nm excitation. (c) The UCL integral intensities and contrast of the above core/shell/shell UCNPs. (d) UC emission spectra of $NaYF_4$:0.5%Er (Er), $NaYF_4$:0.5%Er@$NaGdF_4$:2%Yb (Er@Yb), $NaYF_4$:0.5%Er@$NaGdF_4$:2%Yb@$NaYF_4$:1%Er (Er@Yb@Er) under (d) 850 & 1550 nm, (e) 1550 nm excitation. (f) The UCL integral intensities and contrast of the above core, core/shell, and core/shell/shell UCNPs.

$Yb^{3+}$ in the inner shell, and 1 mol% $Er^{3+}$ in the outer shell were obtained, which exhibits the highest emission intensity and contrast (Fig. 6d and e). In the case of excitation at 850 & 1550 nm, the UCL intensity and contrast of $NaYF_4$:0.5%Er@$NaGdF_4$:2%Yb@$NaYF_4$:1%Er UCNPs were about 3.4 and 2.8 times higher than those of $NaYF_4$:0.5%Er, respectively (Fig. 6f). These results show that the designed core/shell/shell nanostructure significantly enhances TSTF UCL intensities and contrast.

To describe the good performance of the core/shell/shell nanostructure that we designed, a series of measurements were carried out. First, the emission spectra of $NaYF_4$:Er and $NaYF_4$:Yb,Er UCNPs were measured to compare their TSTF UCL intensities and contrasts. As shown in Fig. S6a–c (ESI†), with an increase in $Yb^{3+}$ ion concentration, the UCNPs exhibited higher UCL intensity and lower contrast. In addition, the calculated quantum yields (QY) of core, core/shell and core/shell/shell UCNPs under 1550 nm excitation are $1.73 \times 10^{-8}$, $1.11 \times 10^{-7}$ and $4.58 \times 10^{-8}$, respectively. The changed QY of the as-prepared UCNPs corresponds to the designed nanostructure. With $NaGdF_4$:Yb shell coated, the enhanced UCL intensity in core/shell UCNPs maybe due to the reduction of surface defects and the improvement of absorption at 1550 nm. After $NaYF_4$:Er shell coating, the enhanced UCL contrast in core/shell/shell UCNPs is mainly caused by improving 1550 nm absorption. Finally, we measured the UCL spectra of $NaYF_4$:Er@$NaGdF_4$:Yb@$NaYF_4$:Er and $NaYF_4$:Er@$NaGdF_4$:Yb@$NaYF_4$ UCNPs (Fig. S6d and e, ESI†). The result shows that inactive $NaYF_4$ shell coated onto the $NaYF_4$:Er@$NaGdF_4$:Yb core/shell UCNPs could improve the UCL performance, and the designed nanostructure exhibits better performance. Designing the sensitizer and activator ions in separate layers obtained enhanced UCL intensity and improved contrast.

Under the excitation of an 850 nm laser, no single-frequency UCL was detected in the as-prepared UCNPs. Fixing the 850 nm excitation power at 0.2 W, the 1550 nm laser excitation power gradually increased from 0.2 W to 2.23 W. The TSTF UCL spectra were measured at different 1550 nm excitation powers (Fig. S7a–c, ESI†). As demonstrated in Fig. 7a, it could be observed

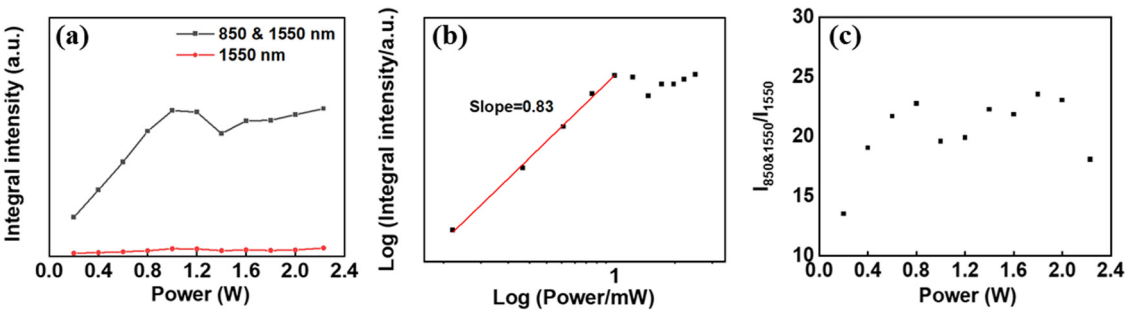


Fig. 7 (a and b) The pump power dependence of UCL integral intensities of $NaYF_4$:0.5%Er@$NaGdF_4$:2%Yb@$NaYF_4$:1%Er UCNPs on 1550 nm laser power. (c) The pump power dependence of UCL contrast on 1550 nm laser power. The 850 nm laser power is maintained at 0.2 W.

that the UCL integral intensities $I_{850\&1550}$ of Er@Yb@Er UCNPs were enhanced with increasing pump power ($P$, 0.2–1 W). In addition, the UCL contrast was also enhanced with increasing pump power (0.2–0.8 W) (Fig. 7c). The result of $I \propto P^{0.83}$ suggests that the emissions under 1550 nm excitation were a single-photon process when the 850 nm excitation power was fixed (Fig. 7b). Therefore, the UC emission was a two-photon process at the excitation of 850 & 1550 nm.

Fig. 8 illustrates the possible energy transfer process of Er@Yb@Er UCNPs excited simultaneously by 850 & 1550 nm. There are two possible pathways for UC emission enhancement; in the pathway ①, $Er^{3+}$ ions distributed in the core and outer shell are first promoted from the $^4I_{15/2}$ state to $^4I_{13/2}$ state by the 1550 nm excitation, then pumped to $^4S_{3/2}$ state by 850 nm excitation, and finally returned to state $^4I_{15/2}$, emitting green TSTF UCL. Additionally, the introduction of the inner shell reduces the surface defect concentration, decreases the energy transfer probability from $Er^{3+}$ to surface defects and enhances the UCL intensity. In pathway ②, $Yb^{3+}$ ions doped in the inner shell played a significant role in promoting the absorption of 1550 nm excitation. The new processes could be described as $^4I_{11/2}$ ($Er^{3+}$) + $^2F_{7/2}$ ($Yb^{3+}$) → $^4I_{15/2}$ ($Er^{3+}$) + $^2F_{5/2}$ ($Yb^{3+}$), $^4I_{15/2}$ ($Er^{3+}$) + $^2F_{5/2}$ ($Yb^{3+}$) → $^4I_{11/2}$ ($Er^{3+}$) + $^2F_{7/2}$ ($Yb^{3+}$), $^4I_{11/2}$ ($Er^{3+}$) → $^4I_{13/2}$ ($Er^{3+}$). These $Er^{3+}$ → $Yb^{3+}$ → $Er^{3+}$ energy transfer processes increase the population of $^4I_{13/2}$ ($Er^{3+}$) level, thereby harvesting the absorption of 1550 nm.

The emission time–decay curves of 542 nm UC emission for the C, C@S and C@S@S UCNPs were measured at the excitation of 1550 nm. (Fig. S8, ESI†). The corresponding lifetimes of possible energy transfer processes ① and ② are $\tau_1$ and $\tau_2$, respectively. With $NaGdF_4$:Yb and $NaYF_4$:Er shells covered, the lifetime $\tau_1$ and $\tau_2$ of 542 nm UC emission increased, which was mainly due to the reduction of energy transfer between $Er^{3+}$ ions and surface defects. The doped $Yb^{3+}$ ions harvest the absorption of 1550 nm (Fig. S9, ESI†). The results agreed well with the assumed transition processes.

Fig. 9a, b and c show the TSTF UCL photographs of core/shell/shell UCNPs solution. Excited by 850 & 1550 nm, the green TSTF UC emission can be detected in $NaYF_4$:0.5%Er UCNPs (Fig. 9a). After the $NaGdF_4$:Yb shell is covered, the

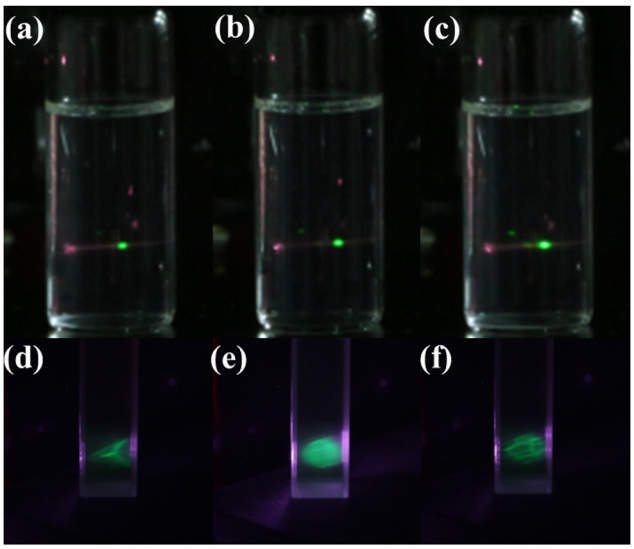


Fig. 9 The TSTF UCL photographs of (a) $NaYF_4$:0.5%Er, (b) $NaYF_4$:0.5%Er@$NaGdF_4$:2%Yb and (c) $NaYF_4$:0.5%Er@$NaGdF_4$:2%Yb@$NaYF_4$:1%Er UCNPs. 3-D image of (d) triangular pyramid, (e) sphere and (f) hollow dodecahedron of $NaYF_4$:0.5%Er@$NaGdF_4$:2%Yb@$NaYF_4$:1%Er UCNPs under 850 & 1550 nm excitation.

$NaYF_4$:0.5%Er@$NaGdF_4$:2%Yb UCNPs possess a higher UC emission (Fig. 9b). Inspiringly, the strongest UCL was observed in resulting $NaYF_4$:0.5%Er@$NaGdF_4$:2%Yb@$NaYF_4$:1%Er UCNPs (Fig. 9c). The enhanced UCL of these UCNPs is consistent with their emission spectra shown in Fig. 6d, significantly supporting the strategy of enhancing TSTF UCL by core/shell/shell nanostructure.

For further application in a 3-D display, a confirmatory experiment was carried out. As shown in Fig. 9d–f, the triangular pyramid, sphere and hollow dodecahedron 3-D images with high resolution were successfully displayed in the as-prepared core/shell/shell UCNPs solution. Moreover, under the same experimental conditions, the Er@Yb@Er and Er@Er@Yb UCNPs with different contrasts were used to display the same 3-D cube (Fig. S10, ESI†). Compared with Er@Er@Yb UCNPs, the higher contrast Er@Yb@Er UCNPs had a better display effect, reasonably.

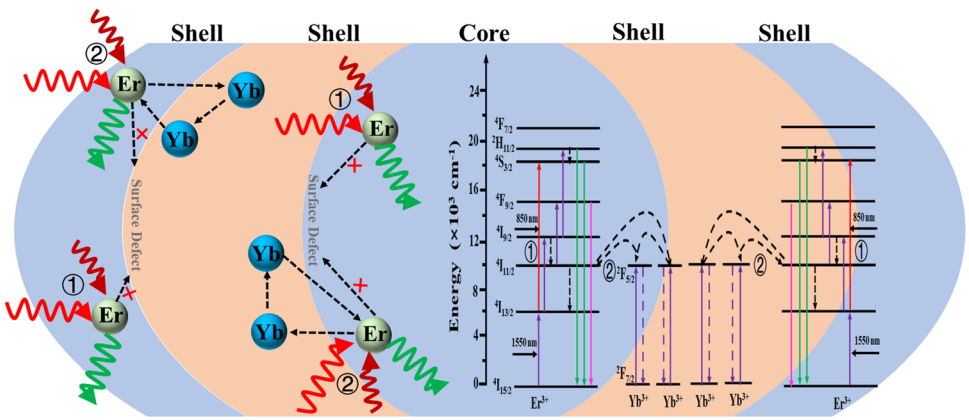


Fig. 8 Schematic illustration of possible energy transfer processes in the core/shell/shell nanostructure.

The above 3-D images demonstrate the great prospects of core/shell/shell UCNPs in the volumetric 3-D display.

## Conclusions

In conclusion, a designed core/shell/shell (Er@Yb@Er) nanostructure was employed to enhance TSTF UCL performance. After optimizing the doping ratio of $Er^{3+}$ and $Yb^{3+}$ ions in this nanostructure, UCNPs with 0.5 mol% $Er^{3+}$ in the core, 2 mol% $Yb^{3+}$ in the inner shell and 1 mol% $Er^{3+}$ in the outer shell exhibited enhanced TSTF UCL performance. In the case of excitation at 850 & 1550 nm, the UCL intensity and contrast of core/shell/shell UCNPs were about 3.4 and 2.8 times higher than those of core UCNPs. This designed nanostructure protects the UCNPs from surface quenching and reduces the concentration quenching of $Er^{3+}$ ions. In particular, the doped $Yb^{3+}$ ions play a promoting role in raising the absorption of 1550 nm. This designed core/shell/shell nanostructure could provide new insights into enhancing TSTF UCL performance and could offer potential applications in the volumetric 3-D display.

## Conflicts of interest

There are no conflicts to declare.

## Acknowledgements

This work was supported by the National Natural Science Foundation of China (11704003).

## References

1 C. Fuchtbauer, *Z. Phys.*, 1920, **21**, 635–638.
2 R. W. Wood, *Proc. R. Soc. London*, 1924, **106**, 679–694.
3 D. R. Gamelin and H. U. Gudel, *Top. Curr. Chem.*, 2001, **214**, 1–56.
4 K. Langhans, C. Guill, E. Rieper, K. Oltmann and D. Bahr, *Proc. SPIE*, 2003, **5006**, 161–174.
5 J. D. Lewis, C. M. Verber and R. B. McGhee, *IEEE Trans. Electron Devices*, 1971, **18**, 724–732.
6 E. Downing, L. Hesselink, J. Ralston and R. Macfalane, *Science*, 1996, **273**, 1185–1189.
7 M. R. Brown and G. S. Waters, *US Pat.*, US3474248A, 1969.
8 X. Chen and Z. Song, *Sci. China, Ser. G: Phys., Mech. Astron.*, 2006, **49**, 169–177.
9 H. H. Refai, *J. Disp. Technol.*, 2009, **5**, 391–397.
10 H. H. Refai, *J. Soc. Inf. Disp.*, 2010, **18**, 1065–1070.
11 J. Dou and Y. Hou, *Chin. J. Lumin.*, 2008, **29**, 85–88.
12 D. C. Nguyen, G. E. Faulkner and M. Dulick, *Appl. Opt.*, 1989, **28**, 3553–3555.
13 A. C. Tropper, J. N. Carter, R. Lauder, R. D. T. Lauder, D. C. Hanna, S. T. Davey and D. Szebesta, *J. Opt. Soc. Am. B*, 1994, **11**, 886–893.
14 O. Henderson-Sapir, J. Munch and D. J. Ottaway, *Opt. Lett.*, 2014, **39**, 493–496.
15 J.-C. G. Bünzli, *Chem. Rev.*, 2010, **110**, 2729–2755.
16 Y. Chen, W. He, Y. Jiao, H. Wang, X. Hao, J. Lu and S. Yang, *J. Lumin.*, 2012, **132**, 2247–2250.
17 J. Zhou, J. Deng, H. Zhu, X. Chen, Y. Teng, H. Jia, S. Xu and J. Qiu, *J. Mater. Chem. C*, 2013, **1**, 8023–8027.
18 Y. Liu, Y. Lu, X. Yang, X. Zheng, S. Wen, F. Wang, X. Vidal, J. Zhao, D. Liu, Z. Zhou, C. Ma, J. Zhou, J. A. Piper, P. Xi and D. Jin, *Nature*, 2017, **543**, 229–233.
19 A. C. Traub, *Appl. Opt.*, 1967, **6**, 1085–1087.
20 D. Perkins, *Space/Aeronaut.*, 1963, 64–67.
21 J. L. Coddington and R. J. Schipper, *SPIE MILESTONE SERIES MS*, 2001, vol. 162, pp. 350–357.
22 A. W. Lohmann and D. Paris, *Appl. Opt.*, 1967, **6**, 1739–1748.
23 B. Lee, *Phys. Today*, 2013, **66**, 36.
24 R. Zito Jr, *J. Appl. Phys.*, 1963, **34**, 1535–1543.
25 R. Barnes, C. Moeller, J. Kircher and C. Verber, *Appl. Phys. Lett.*, 1974, **24**, 610–612.
26 E. A. Downing and B. Torres, *US Pat.*, US4870485A, 1989.
27 I. I. Kim, E. Korevaar and H. Hakakha, *Proc. SPIE.*, 1996, **2650**, 274–284.
28 K. Langhans, C. Guill, E. Rieper, K. Oltmann and D. Bahr, *Proc. SPIE*, 2003, 161–174.
29 J. Allain, M. Monerie and H. Poignant, *Electron. Lett.*, 1991, **27**, 189–191.
30 M. A. Dugay, J. A. Giordmaine and P. M. Rentzepis, *US Pat.*, US3541542, 1970.
31 X. Chen, Y. Feng, G. Zhang, M. Li, K. Li, F. Song, S. Bi, M. Shang, Z. Song, Y. Sun, S. Feng, J. Xiong, C. He, X. Liu and Z. Zheng, *Proc. SPIE.*, 1998, **3560**, 122–131.
32 X. Chen and Z. Song, *Sci. China, Ser. G: Phys., Mech. Astron.*, 2006, **49**, 169–177.
33 J. Dou and Y. Hou, *Chinese J. Lumin.*, 2008, **29**, 85–88.
34 J. H. Cho, M. Bass and H. P. Jenssen, *J. Soc. Inf. Disp.*, 2007, **15**, 1029–1036.
35 M. Bass and H. Jennsen, *US Pat.*, US06501590B2, 2001.
36 R. Deng, F. Qin, R. Chen, W. Huang, M. Hong and X. Liu, *Nat. Nanotechnol.*, 2015, **10**, 237–242.
37 P. Chen, S. Yu, B. Xu, J. Wang, X. Sang, X. Liu and J. Qiu, *Mater. Lett.*, 2014, **128**, 299–302.
38 Y. Li, Z. Li, L. Guo, B. Yang and T. Li, *J. Alloys Compd.*, 2020, **847**, 156399.
39 Y. Li, L. Guo and B. Yang, *Dalton Trans.*, 2021, **50**, 2112–2122.
40 T. J. de Prinse, A. Karami, J. E. Moffatt, T. B. Payten, G. Tsiminis, L. Da Silva Teixeira, J. Bi, T. W. Kee, E. Klantsataya, C. J. Sumby and N. A. Spooner, *Adv. Opt. Mater.*, 2021, **9**, 2001903.
41 X. Zhao, Z. Wu, Z. Yang, X. Yang, Y. Zhang, M. Yuan, K. Han, C. Song, Z. Jiang, H. Wang, S. Li and X. Xu, *Nanomaterials*, 2020, **10**, 1475.
42 M. Tan, M.-J. Monks, D. Huang, Y. Meng, X. Chen, Y. Zhou, S.-F. Lim, C. Würth, U. Resch-Genger and G. Chen, *Nanoscale*, 2020, **12**, 10592–10599.
43 M. Quintanilla, E. Hemmer, J. Marques-Hueso, S. Rohani, G. Lucchini, M. Wang, R. R. Zamani, V. Roddatis, A. Speghini, B. S. Richards and F. Vetrone, *Nanoscale*, 2022, **14**, 1492–1504.
44 Y. Zhang, X. Zhu and Y. Zhang, *ACS Nano*, 2021, **15**, 3709–3735.

45 B. Zhou, L. Yan, J. Huang, X. Liu, L. Tao and Q. Zhang, *Nat. Photonics*, 2020, **14**, 760–766.
46 R. A. Janjua, O. Iqbal, M. A. Ahmed, A. A. Al-Kahtani, S. Saeed, M. Imran and A. G. Wattoo, *RSC Adv.*, 2021, **11**, 20746–20751.
47 X. Qin and X. Liu, *Nanoscale*, 2021, **13**, 19561–19567.
48 X. Zhu, H. Zhang and F. Zhang, *ACS Mater. Lett.*, 2022, **4**(9), 1815–1830.
49 N. Kang, J. Zhao, Y. Zhou, C. Ai, X. Wang and L. Ren, *Nanotechnology*, 2019, **30**, 105701.
50 F. Zhang, R. Che, X. Li, C. Yao, J. Yang, D. Shen, P. Hu, W. Li and D. Zhao, *Nano Lett.*, 2012, **12**, 2852–2858.
51 B. Chen and F. Wang, *Trends Chem.*, 2020, **2**, 427–439.
52 N. Dubey and S. Chandra, *J. Rare Earths*, 2022, **40**, 1343–1359.
53 B. Zheng, J. Fan, B. Chen, X. Qin, J. Wang, F. Wang, R. Deng and X. Liu, *Chem. Rev.*, 2022, **122**, 5519–5603.
54 B. Zhou, B. Tang, C. Zhang, C. Qin, Z. Gu, Y. Ma, T. Zhai and J. Yao, *Nat. Commun.*, 2020, **11**, 1174.
55 P. Huang, W. Zheng, S. Zhou, D. Tu, Z. Chen, H. Zhu, R. Li, E. Ma, M. Huang and X. Chen, *Angew. Chem., Int. Ed.*, 2014, **53**, 1252–1257.
56 M. G. Ding, D. Q. Chen, D. Y. Ma, J. N. Dai, Y. T. Lia and Z. G. Jia, *J. Mater. Chem. C*, 2016, **4**, 2432–2437.
57 D. Li, S. Wen, M. Kong, Y. Liu, W. Hu, B. Shi, X. Shi and D. Jin, *Anal. Chem.*, 2020, **92**, 10913–10919.
58 Y. Zhou, Y. Cheng, J. Xu, H. Lin and Y. Wang, *Nanoscale*, 2021, **13**, 6569–6576.
59 C. Lin, Z. Xia, L. Zhang, X. Chen, Q. Sun, M. Lu, Z. Yuan, X. Xie and L. Huang, *ACS Appl. Mater. Interfaces*, 2020, **12**, 31783–31792.
60 S. Wen, D. Li, Y. Liu, C. Chen, F. Wang, J. Zhou, G. Bao, L. Zhang and D. Jin, *J. Phys. Chem. Lett.*, 2022, **13**, 5316–5323.
61 D. Chen, P. Huang, Y. Yu, F. Huang, A. Yang and Y. Wang, *Chem. Commun.*, 2011, **47**, 5801–5803.
62 F. Wang, Y. Han, C. Lim, Y. Lu, J. Wang, J. Xu, H. Chen, C. Zhang, M. Hong and X. Li, *Nature*, 2010, **463**, 1061–1065.